Naval Research Laboratory

Washington, DC 20375-5320

NRL/MR/6795--97-7947

Precursor-Shock in a Well-Characterized Thermal Layer

J. GRUN
R. BURRIS
G. JOYCE
S. SLINKER
J. HUBA

Beam Physics Branch
Plasma Physics Division

K. EVANS

Sachs Freeman Associates
Landover, Maryland

C.K. MANKA

Research Support Instruments
Lanham, Maryland

J.R. BARTHEL

Maxwell Laboratories, Inc.
La Jolla, California

December 22, 1997

REPORT DOCUMENTATION PAGE

Form Approved
OMB No. 0704-0188

1. AGENCY USE ONLY (*Leave Blank*)	2. REPORT DATE	3. REPORT TYPE AND DATES COVERED
	December 22, 1997	Interim Report

4. TITLE AND SUBTITLE

Precursor-Shock in a Well-Characterized Thermal Layer

5. FUNDING NUMBERS

6. AUTHOR(S)

J. Grun, R. Burris, G. Joyce, S. Slinker, J. Huba, K. Evans,* C.K. Manka,†
and J.R. Barthel‡

7. PERFORMING ORGANIZATION NAME(S) AND ADDRESS(ES)

Naval Research Laboratory
Washington, DC 20375-5320

8. PERFORMING ORGANIZATION REPORT NUMBER

NRL/MR/6795--97-7947

9. SPONSORING/MONITORING AGENCY NAME(S) AND ADDRESS(ES)

Defense Special Weapons Agency
Alexandria, VA 22310-3398

10. SPONSORING/MONITORING AGENCY REPORT NUMBER

11. SUPPLEMENTARY NOTES

*Sachs Freeman Associates, Landover, MD 20785
†Research Support Instruments, Lanham, MD 20796
‡Maxwell Laboratories, Inc., La Jolla, CA 92038

12a. DISTRIBUTION/AVAILABILITY STATEMENT

Approved for public release; distribution unlimited.

12b. DISTRIBUTION CODE

13. ABSTRACT (*Maximum 200 words*)

We present an experiment that measured the behavior of a shock precursor in a well-characterized, thin thermal layer above a 3000°K hot surface. A laser pulse focused onto a thin solid target produced the shock, eliminating interference from explosion products. Precursor and thermal layer characteristics were measured using spectroscopy, interferometry, and dark-field shadowgraphy.

14. SUBJECT TERMS

Precursor
Shock
Thermal layer

15. NUMBER OF PAGES

28

16. PRICE CODE

17. SECURITY CLASSIFICATION OF REPORT	18. SECURITY CLASSIFICATION OF THIS PAGE	19. SECURITY CLASSIFICATION OF ABSTRACT	20. LIMITATION OF ABSTRACT
UNCLASSIFIED	UNCLASSIFIED	UNCLASSIFIED	UL

NSN 7540-01-280-5500

Standard Form 298 (Rev. 2-89)
Prescribed by ANSI Std 239-18
298-102

PRECURSOR-SHOCK IN A WELL-CHARACTERIZED THERMAL LAYER

A *thermal shock precursor* forms when a shock wave propagating through ambient air encounters a layer of hot gas whose sound speed is higher than the sound speed in the ambient. Precursor formation begins when a portion of the incident shock wave refracts into the hot layer creating a toe wave that accelerates ahead of the main shock and increases the static pressure in the shocked hot gas (Figure 1). In turn, this increased pressure drives a shock - the precursor – back into the ambient air. When the precursor encounters the original shock wave, a reflected shock propagating into the hot layer is formed. The interaction of this reflected shock with the hot gas layer generates vortical flow that sweeps additional air into the layer and reinforces the toe wave further to complete the cycle. Precursor shocks, which were first observed in nuclear explosions as early as Trinity,[1] are thought to play a role during explosive breakup of meteorites in the atmosphere, high-velocity impact of cosmic bodies on planetary surfaces, and in the interaction of interplanetary shocks with the geomagnetic tail.[2,3] Some have even suggested harnessing artificially induced precursors to alter the trajectories of small but dangerous asteroids entering the earth's atmosphere.[4]

Very few experiments have measured precursor formation in well-characterized thermal layers.[5] Most published results considered precursors near the interface of two gas layers stacked above a plane surface.[6] The gas closer to the surface had a higher sound speed and, therefore, served as a model of a thermal layer. However, the two gases in some experiments were kept apart by a plastic sheet, which may have affected precursor dynamics. Also, in these experiments the density profile of the higher-sound-

Manuscript approved August 28, 1997

speed gas either decreased away from the surface or was uniform, a situation unlike the density profile of a thermal layer in which the surface is the source of heat. In thermal layers the gas density is lowest near the surface where the temperature is highest.

In this paper, we describe an experiment that measured the characteristics of a precursor in a well-characterized, thin thermal layer produced by the rapid heating of a metal foil. The brightness temperature of the hot surface was measured spectroscopically. Density and temperature profiles of the thermal layer, as well as the density within the shock and the precursor, were determined using Abel-inverted interferographs. Dark-field shadowgraphs, acquired simultaneously with the interferographs, measured the propagation characteristics of the shock and precursor.

A laser pulse focused onto a thin solid target produced the main shock wave in our experiment. Shocks produced by laser pulses were proven to behave like ideal Taylor-Brode-Sedov shocks generated by more conventional means such as explosions or shock tubes.[7,8,9] However, laser-generation of shocks has a number of advantages. Pressures achieved with laser-induced shocks can be much higher than pressures achievable with either chemical explosives or shock tubes.[9] Moreover, since a laser-explosion has little mass, the shock can be observed for a long time without being overrun by explosion products.

The experiment took place inside an aluminum box of ~ 15-cm length per side (Figure 2). A hollow cone positioned with its apex protruding into the box was attached to one of the box walls. The cone's tip was cut off leaving a 1-mm diameter opening that was closed by a 2.5-μm thick layer of mylar. Inside the box was a 5 cm x 5 cm x 12 μm tantalum sheet oriented with its surface perpendicular to the cone axis and attached in series to a switched 780-μf external capacitor charged by a 1.3-kV power supply. The distance between the cone tip and the tantalum sheet was adjustable from zero to 3 cm. Glass windows on the box's two opposite walls allowed viewing and access to optical diagnostics.

To produce a precursor shock the box was first placed inside a larger vacuum chamber, both the box and the chamber were evacuated, and the box was back-filled with one atmosphere of argon gas. The capacitor was then discharged through the tantalum foil, heating the foil and a thin layer of argon gas above it. (The parameters of the discharge circuit were chosen to generate a fast-rising current that heated the foil quickly so that the layer of gas above the tantalum remained thin and laminar for the duration of the experiment. See Figure 3a.) One millisecond later the laser was fired to produce a shock. The laser, a 130-joule, 1.054-μm, 5-ns duration pulse, was focused through the vacuum of the larger chamber onto the tip of the cone where it irradiated and rapidly heated the mylar foil. The heated mylar expanded rapidly, much like the products of a chemical explosion, forming a shock in the argon gas that propagated into the box and through the thermal layer above the heated tantalum sheet.

The heated tantalum reached brightness temperatures as high as 3000°K (Figure 3b). The temperature and its time-evolution were determined by a grey-body fit to light emission from the tantalum surface, spectrally resolved from 500-700 nm and recorded with a streak camera. The light emission rose to a maximum in 40 μsec, together with the current, and remained constant within 13% for 1 msec. We estimated that a 13% emission variation corresponds to a temperature variation of less than 2%. The imaging system was calibrated between 1500 and 2800°K using a tungsten lamp with emission characteristics traceable to the National Bureau of Standards. We also used the tungsten lamp to test the sensitivity of the fitting and data reduction procedure, from which we estimated that, despite the small wavelength range measured, temperatures that differ by 6% could be distinguished. Light emission from the tantalum was also monitored on each calibration shot with an MRD 510 photodiode sensitive from 400 to 1100 nm. Emission in this visible to near-IR band was correlated with foil temperatures determined spectroscopically, and the photodiode was used as a temperature monitor on each data shot.

The thermal layer and the shock were probed with a 0.53-μm, 0.35-ns duration, and 5-cm diameter, 50-mJ laser-probe that illuminated the experiment along the surface of the tantalum sheet. Laser probe light passing through the experiment was collected with a telescope, imaged using dark-field-shadowgraphy and recorded with a folded-wave interferometer.[10] The density and temperature profiles of the thermal layer are determined from the probe's phase shift δ given by

(1) $$\frac{\delta(z)}{2\pi} = \frac{1}{\lambda}\int_{-\infty}^{\infty}(n(z)-n_0)ds = (n_0-1)\frac{L}{\lambda}\left(\frac{\rho(z)}{\rho_0}-1\right),$$

where $n_0 = 1.000282$ is the index of refraction of argon at 1 atm. and 0°C, L is the length of the tantalum foil, λ is the probe wavelength and $\rho(z)$ and ρ_0 are gas densities inside and outside the hot layer respectively.[11,12] The letter z designates a direction perpendicular to the tantalum foil surface. In writing this expression we assumed that the index of refraction n is proportional to density with negligible explicit dependence on temperature (i.e. $n = 1 + (n_0\text{-}1)\rho/\rho_0$). In addition, since one millisecond, the time at which the shock wave was initiated, is much larger than the microsecond sound-transit time through the hot layer (~ 1 mm/319 m/sec), the pressure in the hot layer should be equilibrated with the pressure of the rest of the gas. Under these circumstances the temperature $T(z)$ in the layer is related to probe phase through

(2) $$\frac{\delta(z)}{2\pi} = (n_0-1)\frac{L}{\lambda}\left(\frac{T_0}{T(z)}-1\right),$$

where T_O is the temperature of the unheated gas.

Figure 4 presents the temperature profile of the hot layer at one millisecond. During the 30 μsec that the shock wave sweeps over the tantalum foil (as will be shown below) the layer may be taken to be stationary.

Figure 5 through Figure 7 show development of the shocks in our experiment. The principal shock, initiated 11.5 mm above the surface, was first observed at 6.8 μsec when its radius was 17.8 mm: In the subsequent 23.6 μsec it propagated to 32.6 mm. The

precursor, conversely, was 2.5 mm long at 6.8 μsec and developed to a length of 6.6 mm by 17.4 μsec. As in our previous work,[7,8,9] the radius r of the principal shock scales very well as the 2/5th power of time t, in conformance with the Taylor-Brode-Sedov similarity solution for a massless point-source explosion

$$r = \left(\frac{E/\alpha(\gamma)}{\rho_0} \right)^{1/5} t^{2/5}, \tag{3}$$

where E is the explosion energy, ρ_0 is the mass density of the ambient gas, and $\alpha(\gamma)$ is an adiabatic index dependent correction factor related to the efficiency of converting explosion energy to shock energy.[13] If E is identified with the laser energy then an α of 2 is required to fit the absolute r vs. t values to the data, indicating that the post-shock γ is about 1.2 in the experiment.[14] From expressions[13] for shock pressure P and shock velocity $\dot{r}$

$$P = \frac{2}{\gamma+1} \rho_0 \dot{r}^2 [1 - \frac{\gamma-1}{2\gamma} \frac{c^2}{\dot{r}^2}] \tag{4}$$

$$\dot{r} = \frac{2r}{5t} \tag{5}$$

where c, the sound speed in argon at room temperature, is 330 m/sec, we infer that at the first observation the pressure of the principal shock was 13-17 atmospheres, for a pre-shock γ between 5/3 and 1 respectively, and at the last observation 2-3 atmospheres. More precise Hugoniot calculations using the SESAME 5172 equation-of-state table for argon yield pressures very close to those obtained from equation 4 with a pre-shock γ of

5/3: At 6.84 μsec they give a pressure of 13.3 atm, at 21.3 μsec a pressure of 8.4 atm, and at 30.4 μsec a pressure of 2.0 atm.

During the observation period the precursor height defined at the triple point, (where the precursor shock, the main shock, and the reflected shock meet), increased at 190 m/sec, changing from 2.1-mm at 6.8 μsec to 6.6 mm by 30.4 μsec. Interestingly, the ratio of precursor height to main shock radius was not constant, as would be the case if the precursor propagation were self-similar. Rather, the ratio increased in an approximately linear fashion from 0.1 at 6.8 μsec to 0.2 by the end of the experiment.

Theories that describe the formation of a precursor at the interface of two dissimilar gases of density ρ_0 and ρ_a predict that the angle of the precursor with respect to the horizontal (β in Figure 7) is given as $\sin(\beta) = \sqrt{\frac{\rho_a}{\rho_0}}$.[15] It is interesting to apply this expression to our experiment and determine where the analogous densities occur. In our experiment, precursor angle is 24 degrees, which corresponds to a density ratio of 0.17 in the above expression. (The angle may be decreasing slightly from 26 to 23 degrees in time.) The equivalent temperature ratio in our experiment would be 6, which occurs at about 1 mm away from the tantalum surface (Figure 4).

The density profiles inside and outside the shocks are determined from interferometry analyzed using the inverse Abel transform method.[16] The technique is here applied as follows: The fringe shift associated with a ray traversing heated or shocked gas is given by (Figure 8)

(6) $$\frac{\delta(r,z)}{2\pi} = \frac{1}{\lambda}\int_{-\infty}^{\infty}(n(r,z) - n_0(z))ds.$$

Here r is a cylindrical radius extending from the axis of symmetry. If z is above the thermal layer then $n_0(z) = n_0$ is index of refraction of unheated argon. But if z is within the thermal layer, then $n_0(z)$ is index of refraction of the heated but unshocked thermal layer in Figure 4. (An underlying assumption is that the thermal layer is reproducible from shot to shot.) Assuming cylindrical geometry, and noting that $s^2 = r^2 - x^2$, $sds = rdr$, and $ds = rdr / \sqrt{r^2 - x^2}$ (Figure 8), the integration along s in can be rewritten as

(7) $$\frac{\delta(r,z)}{2\pi} = \frac{1}{\lambda}\int_{s}^{\infty}\frac{(n(r,z) - n_0(z))2rdr}{\sqrt{r^2 - x^2}}.$$

Using the Abel transform this expression can be inverted to yield

(8) $$n(r,z) = n_0(z) - \frac{\lambda}{\pi}\int_{r}^{\infty}\frac{d\delta(r,z)}{2\pi dx}\frac{dx}{\sqrt{x^2 - r^2}},$$

which can be numerically solved to determine the index of refraction *n(r,z)*. Furthermore, since

(9) $$n(r,z) = 1 + (n_0(z) - 1)\frac{\rho(r,z)}{\rho_0},$$

the density profile can be determined from

(10) $$\frac{\rho(r,z)}{\rho_0} = 1 - \frac{1}{n_0(z) - 1}\frac{\lambda}{\pi}\int_{r}^{\infty}\frac{d\delta(r,z)}{2\pi dx}\frac{dx}{\sqrt{x^2 - r^2}}.$$

Determination of $\delta(r,z)$ requires a certain amount of caution and judgment since the fringe pattern can be quite complicated as shown in Fig. 5. In some regions of the interferograph it is difficult to clearly identify and associate phases with fringe lines.

The results of the analysis are shown in Figs. 9 through 12. Figures 9 and 10 pertain to the shots with a thermal layer in Figure 5, while Figs. 11 and 12 pertain to the shots without a thermal layer in Figure 6. In Fig. 9 we show grayscale contour plots of the density gradients (left-hand side) and the density ρ/ρ_0 (right-hand side) at 6.8, 10.2, 17.4, and 30.4 μsec. In this figure, dark gray indicates high relative densities, while light gray indicates low relative densities. The thermal layer is analyzed for all the thermal shots except that at 17.4 μsec; only the fringes above the `wave-like' discontinuity in the interferograph at 17.4 μsec in Fig. 5 could be clearly identified and labeled.

The shadowgraphs in Figure 5 compare well to the reconstructed density gradient contours in Figure 9. The major shock structure around the triple point is obtained from the Abel analysis, as well as some of the minor structures (e.g., at 6.8 μsec). One problem, somewhat evident in Figure 9, especially at 6.8 and 30.4 μsec, is a noisy hash seen most clearly in the upper right portions of the density gradient plots. This arises because of the nature of the data and the inverse Abel transform. The integrand of the inverse Abel transform is proportional to $d\delta / dx$; when the data is noisy this can lead to large variations in the slope of δ and hence, noisy results. Some data smoothing is used to mitigate this effect.

The density contours of ρ/ρ_0 in Figure 9 show that the gas undergoes a compression at the shocks and then a subsequent rarefaction (this latter point is most obvious at 6.8 μsec). The amount of compression appears to be a function of relative position to the triple point where the density enhancement is largest. The actual relative density profiles ρ/ρ_0 as a function of radius and height above the plate (z direction) are shown in Figure 10 at 6.8, 10.2, 17.4, and 30.4 μsec. The z-direction in this figure also measures the relative density; the spacing between tick marks is unity. For example, consider the topmost density profile in Figure 10 at 6.8 μsec, which corresponds to the top of the density contour in Figure 9. The gas is undisturbed near the left boundary so that $\rho/\rho_0 = 1$. At the shock, the relative density rapidly increases to slightly more than one unit, so that $\rho/\rho_0 \geq 2$. Continuing downstream of the shock (to the right in the figure), the density ρ/ρ_0 decreases below unity. The maximum density jump obtained from the analysis is $\rho/\rho_0 \cong 2.9$ and occurs at 6.8 μsec. Hugoniot calculations, mentioned earlier, give $\rho/\rho_0 = 3.1$ at 6.8 μsec, $\rho/\rho_0 = 2.7$ at 21.4 μsec, and $\rho/\rho_0 = 1.5$ at 30.4 μsec, which is the same result one would get from the expression[13]

$$\frac{\rho}{\rho_0} = \frac{\gamma+1}{\gamma-1}\left[1+\frac{2}{\gamma-1}\frac{c^2}{\dot{r}^2}\right]^{-1} \tag{11}$$

with $\gamma = 5/3$.

Figures 11 and 12 are similar to Figs. 9 and 10, but are for shots without a thermal layer (see Fig. 6). Because there is no thermal layer, the shock structures are not very

complex. Again, the density gradient contours in Fig. 11 are to be compared with the shadowgraph in Fig. 6. The agreement between the two is good, especially at 17.4 μsec. At 30.4 μsec the shadowgraph (Fig. 6) shows an almost horizontal discontinuity downstream of the triple point. Although there is some indication of this in Fig. 11, it is very weak and comparable to noise levels. The density contours in Fig. 11 also show a strong compression at the shock followed by a rarefaction of the gas. At 17.4 μsec there is a compression and rarefaction associated with the first shock structure, followed by a weaker compression and rarefaction with the second shock structure. These features are also shown in Fig. 12 which is a plot of the relative density profile ρ/ρ_0 as a function of radius and height. The maximum density compression is $\rho/\rho_0 \cong 2.7$ at 17.4 μsec.

The authors would like to thank Mr. Levi Daniels for his technical support and Ms. Naomi Frankel for analyzing some of the data. We are also grateful to Dr. Gary Schneyer of Maxwell Inc. and Mr. Emil Braun of NIST for helpful discussions and suggestions. This work was supported by the Defense Special Weapons Agency.

Figure 1

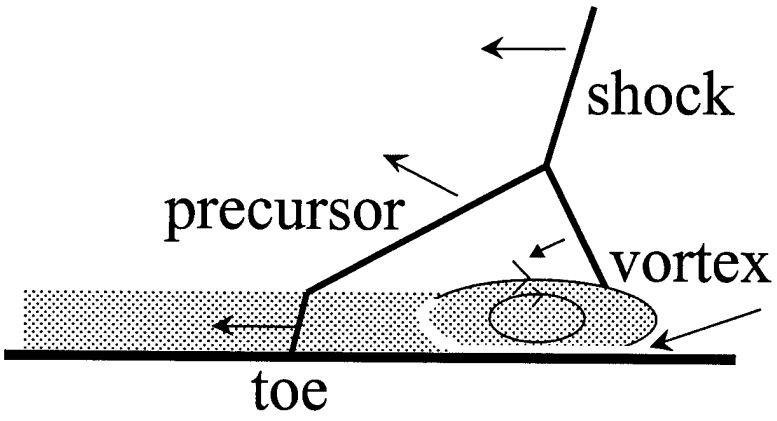

Schematic of precursor shock formation. Shock propagating through air refracts in a thermal layer creating a toe wave that accelerates ahead of the main shock. Increased pressure behind the toe drives a precursor, which upon reflection from the main shock creates a reflected wave that propagates back towards the thermal layer. The interaction of this wave with the thermal layer generates vortical flow that sweeps additional air into the thermal layer and further reinforces the toe.

Figure 2

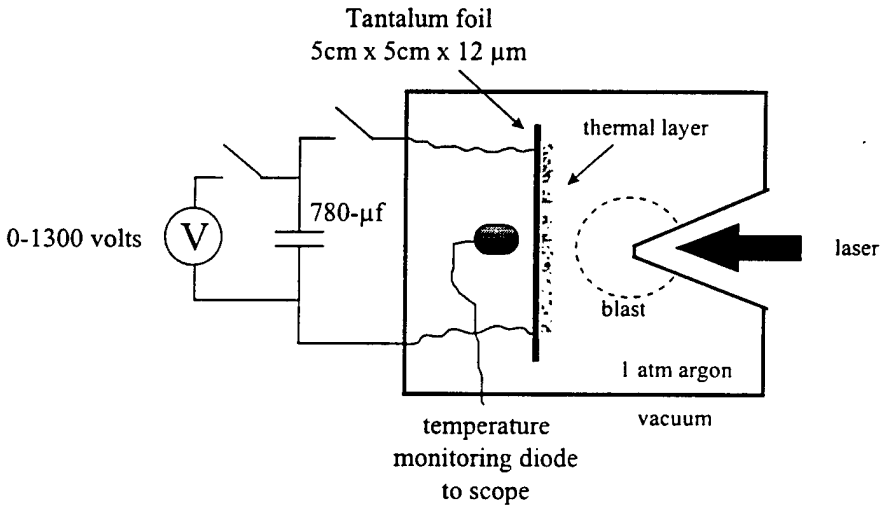

Setup of experiment

Figure 3

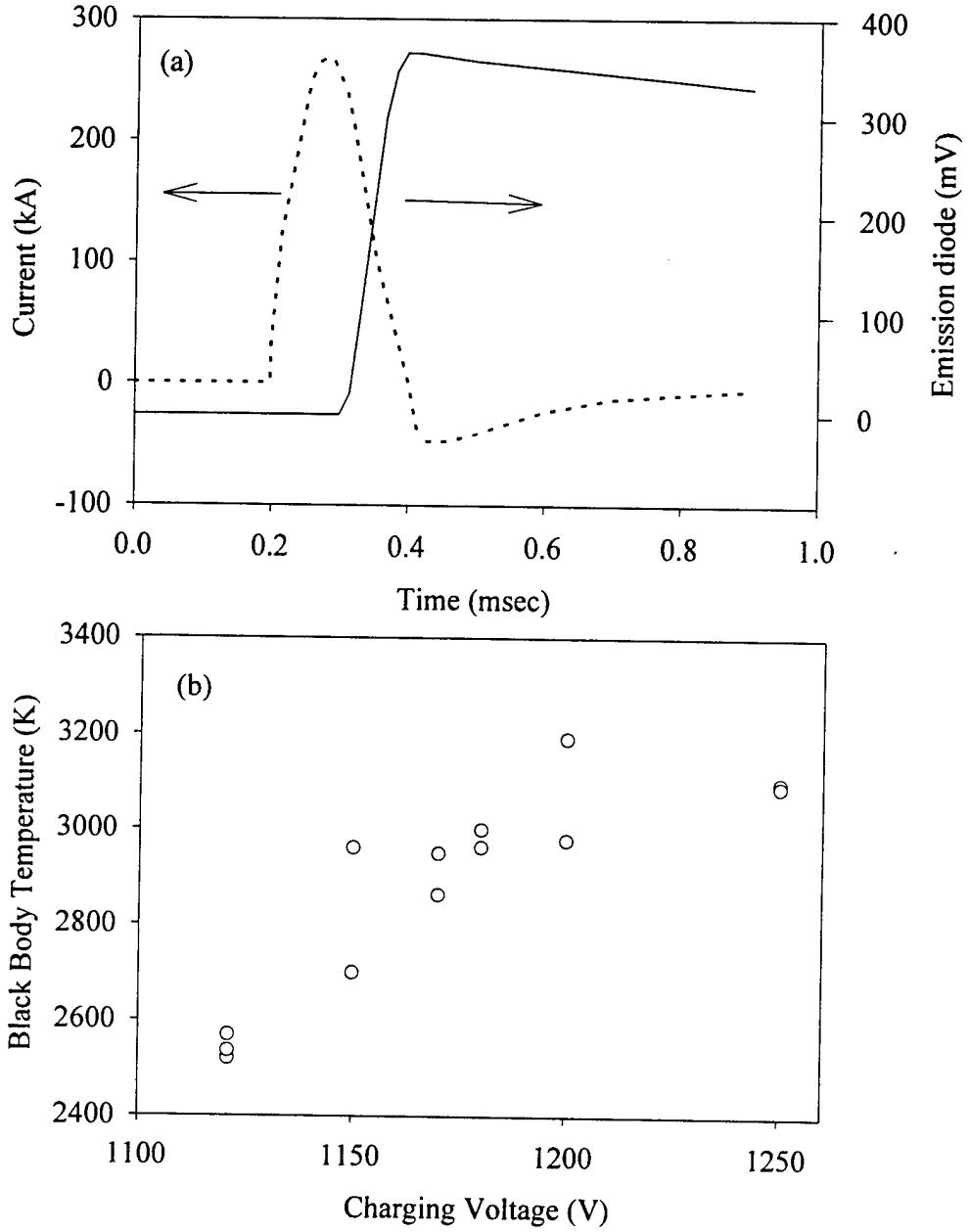

(a) Profiles of the tantalum foil current and the light emission from its surface. (b) Temperature of the tantalum foil vs. charging voltage.

Figure 4

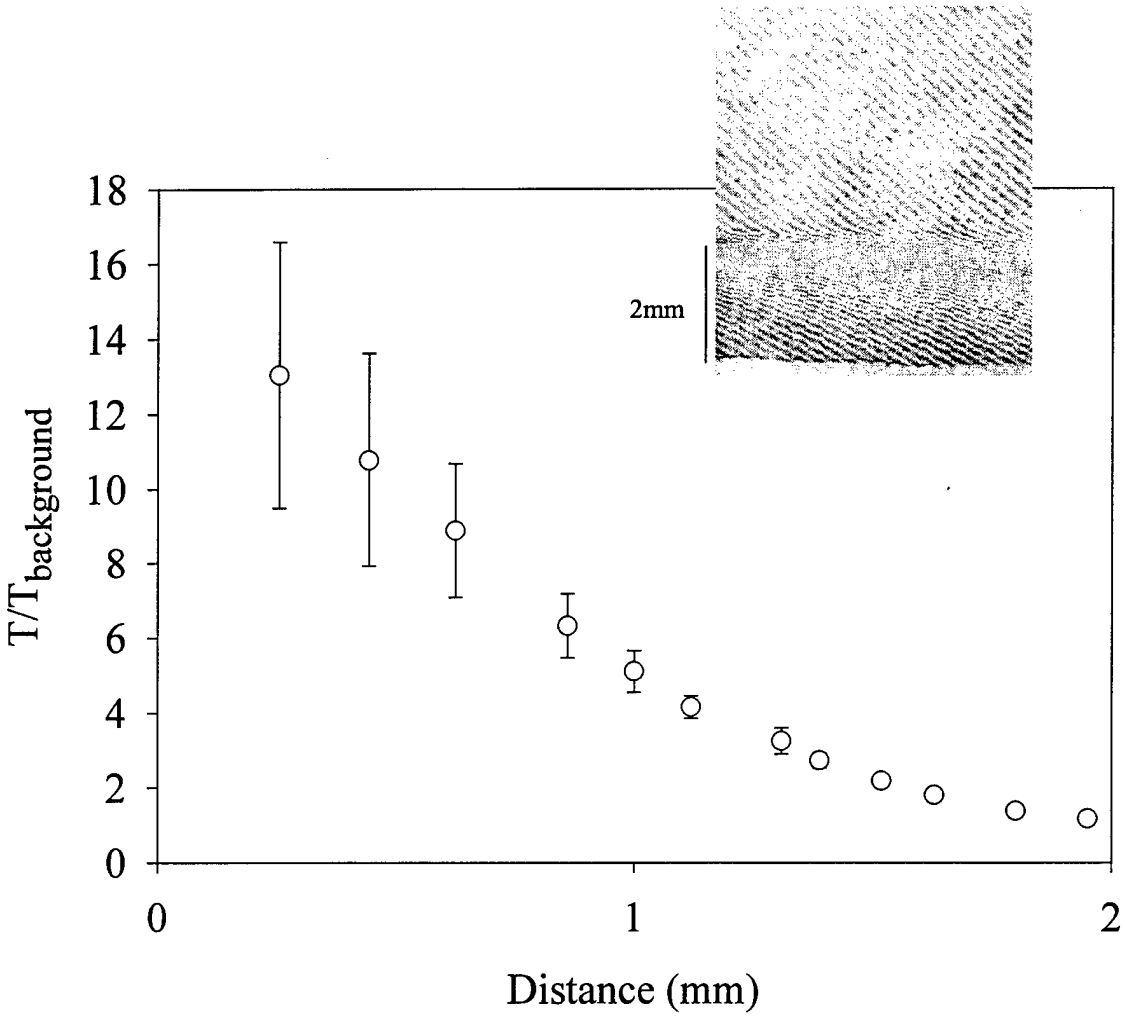

Temperature profile of Argon gas as a function of distance from the tantalum foil at one millisecond. The profile was determined using interferometry (inset). When the temperature is large (and density small) small phase errors translate to large temperature errors.

Figure 5

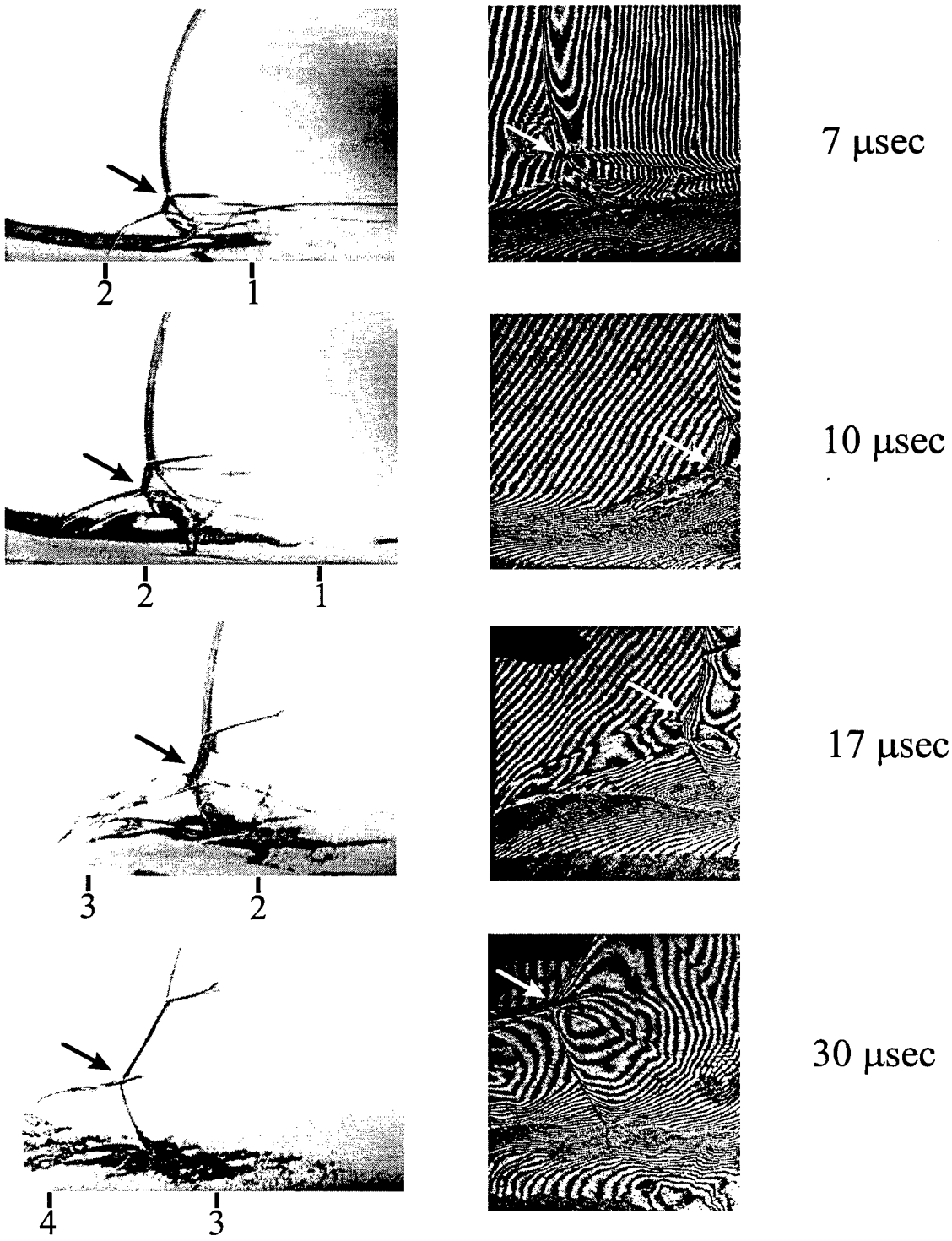

Dark-field shadowgraphs and interferographs showing time-evolution of a precursor shock. Ground range on the shadowgraphs is measured in centimeters. The laser energy was 138, 104, 87, and 137 joules respectively. The blast was initiated 11.5 mm above the surface.

Figure 6

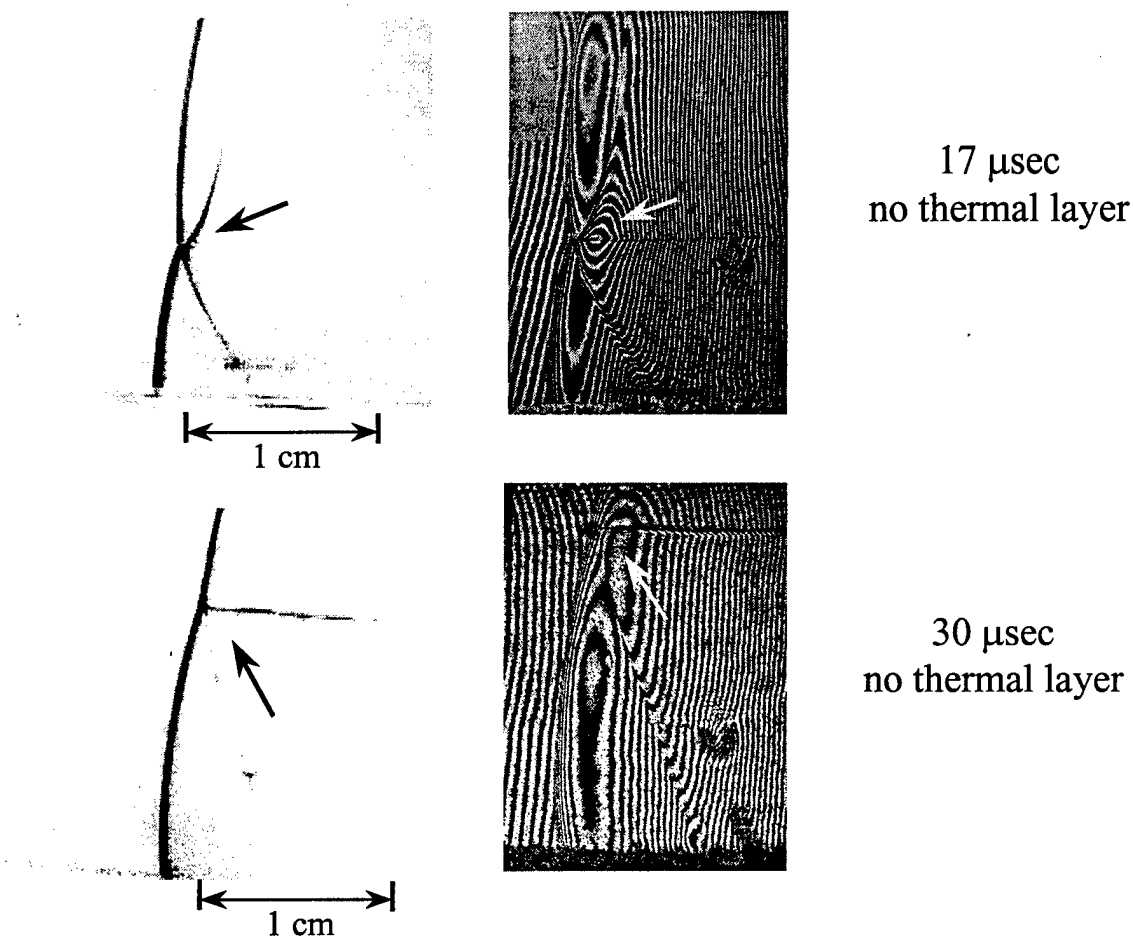

Shocks at 17 μsec and 30 μsec over a surface with no thermal layer. Ground range on the shadowgraphs is measured in centimeters. The laser energy was 83 joules, and 135 joules respectively. The blast was initiated 11.5 mm above the surface.

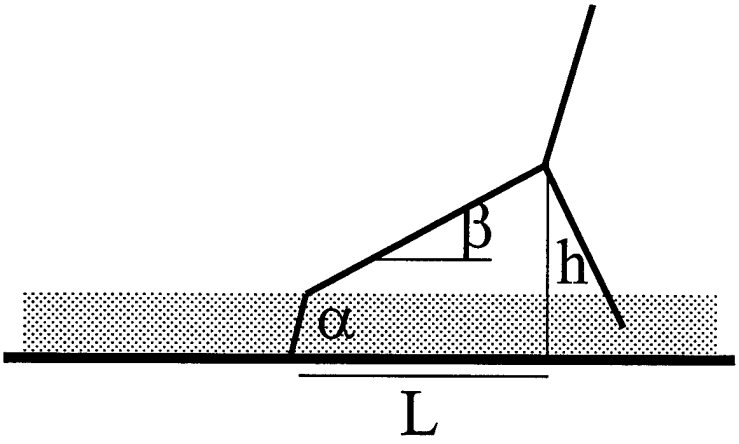

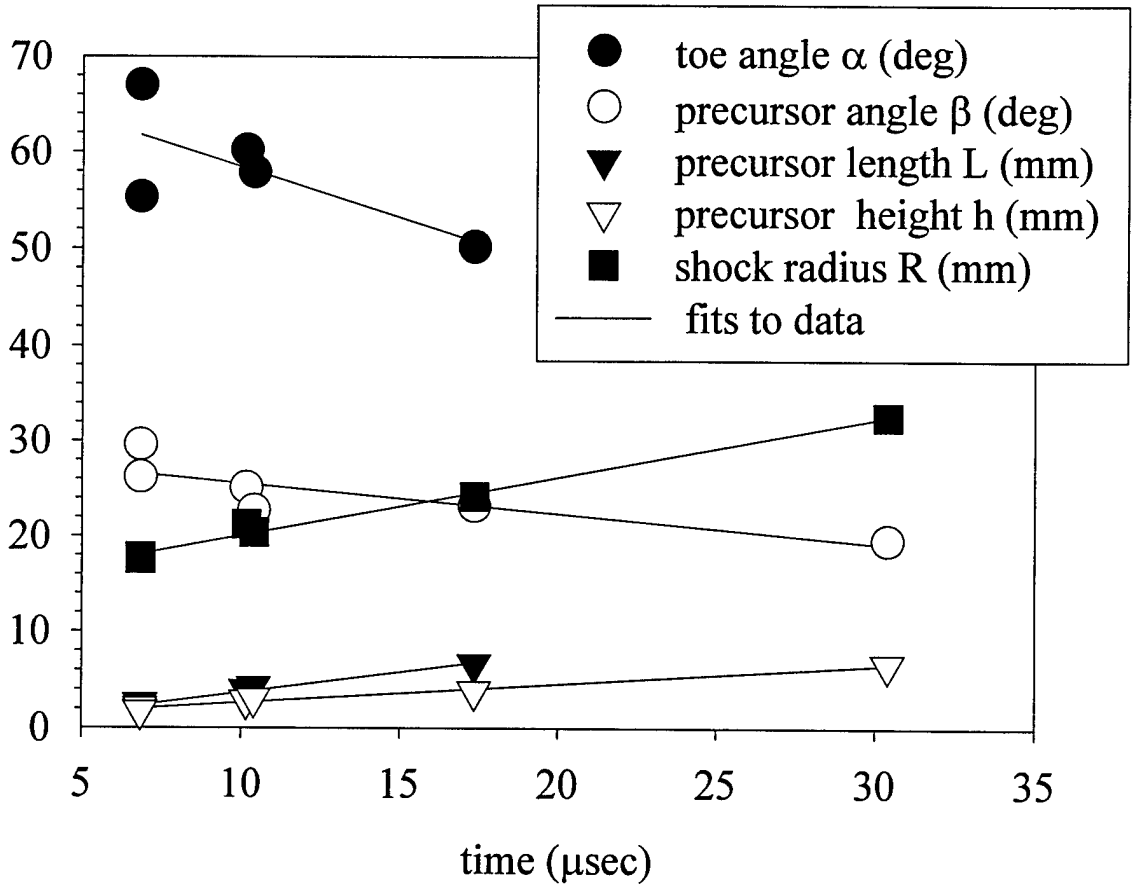

Precursor length and height, and the angles of the precursor and toe shocks with respect to the hot surface.

Figure 8

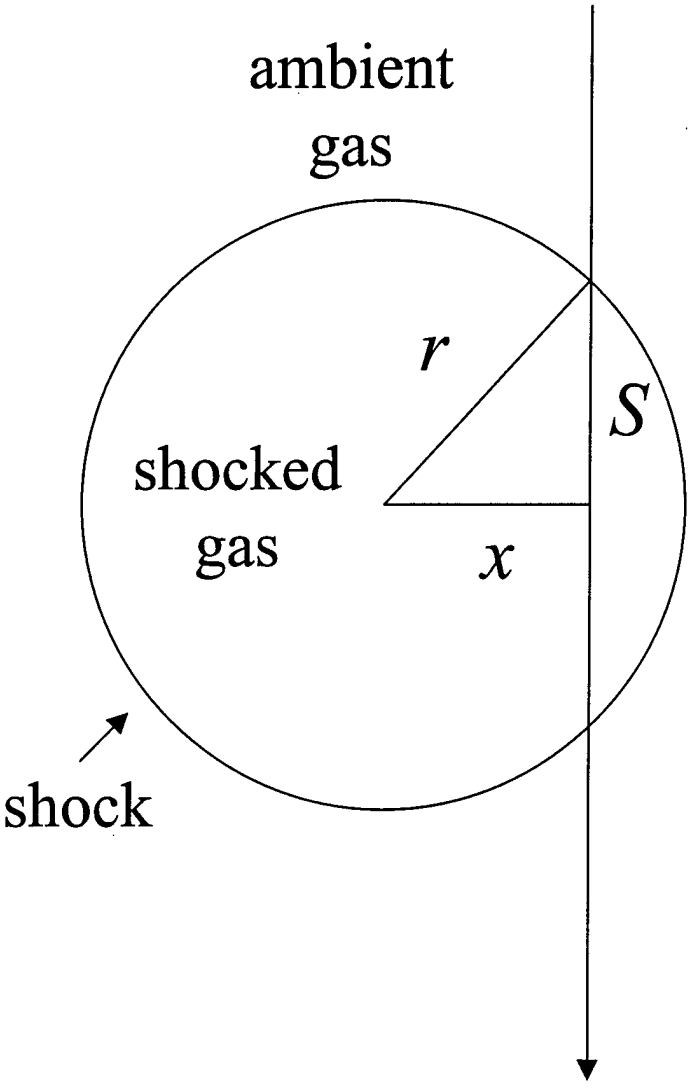

Schematic of ray paths and geometry used in the Abel analysis of the interferographs.

Figure 9

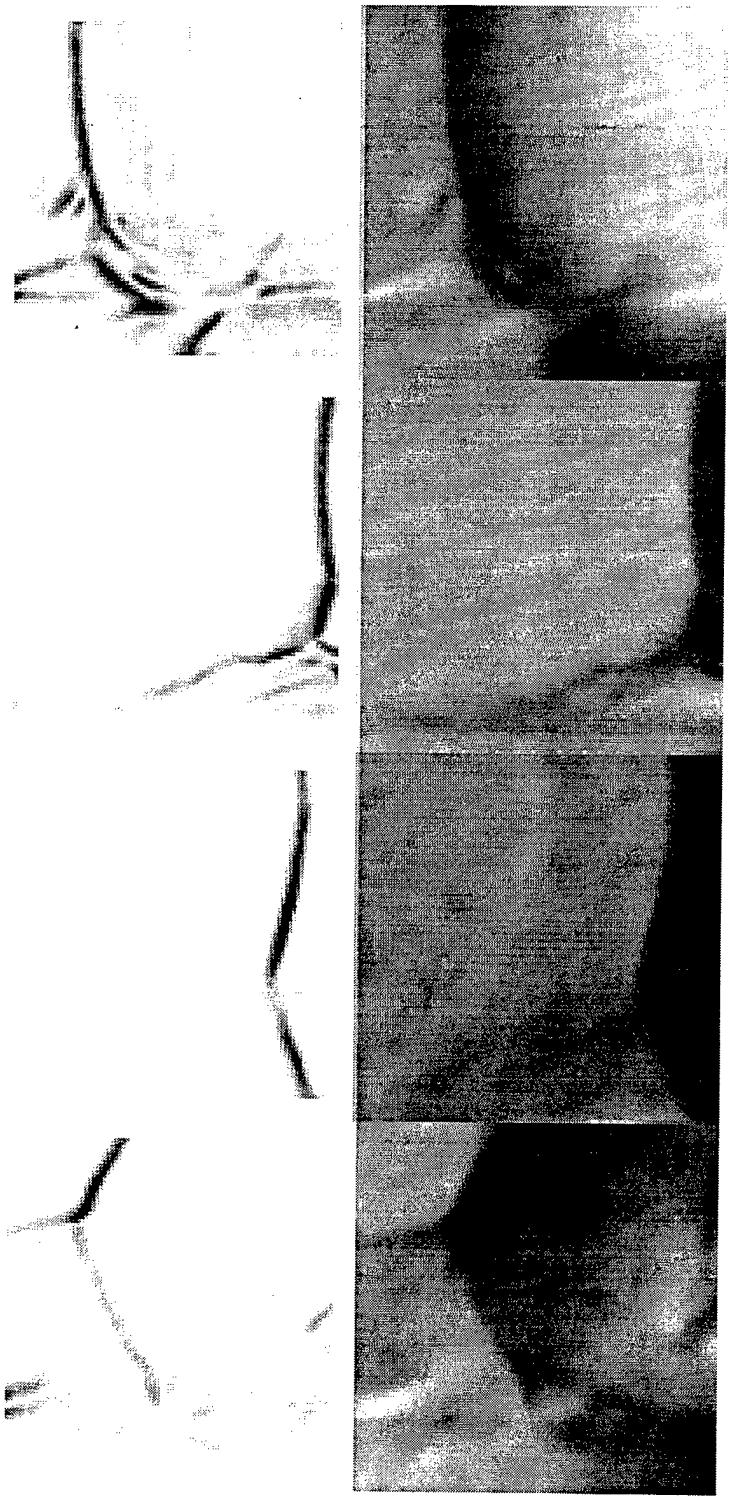

Grayscale contour plots of the density gradients (left hand side) and the density ratio ρ/ρ_0 (right hand side) at 6.8, 10.2, 17.4, and 30.4 μsec for the shots shown in Figure 5. The dark gray indicates high relative densities, while the light gray indicates low relative densities. The density gradient plots are to be compared to the shadowgraphs near the triple point in Figure 5.

Figure 10

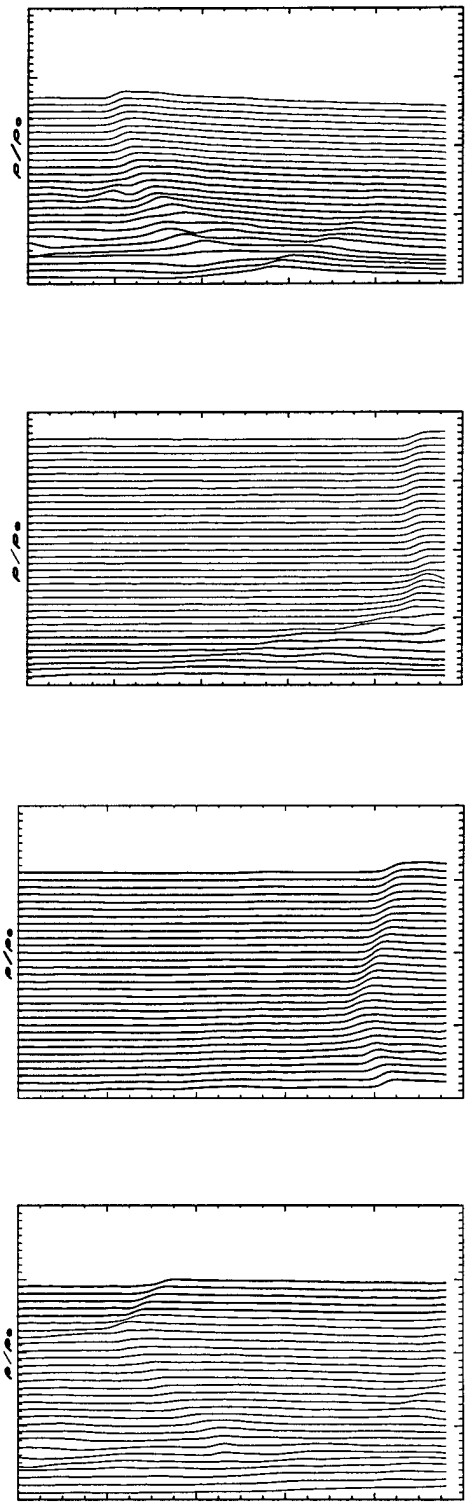

The relative density profiles ρ/ρ_0 as a function of radius (x-axis) and height above the plate (y-axis) at 6.8, 10.2, 17.4, and 30.4 μsec for shots with a thermal layer. The y-axis also measures the relative density; the spacing between tick marks is unity.

Figure 11

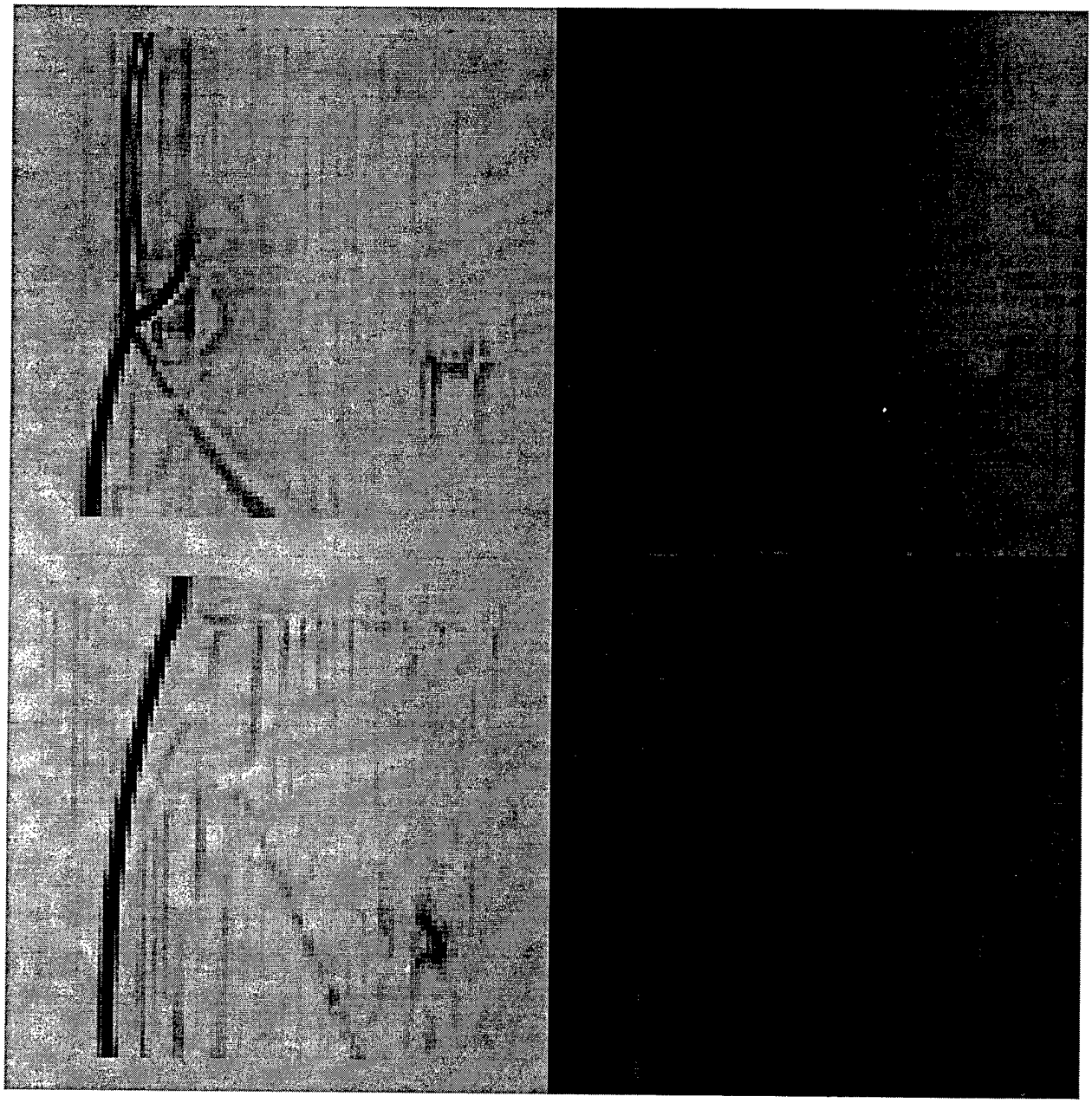

Grayscale contour plots of the density gradients (left hand side) and the density ratio ρ/ρ_0 (right hand side) at 17 and 30 μsec for shots without a thermal layer shown in Figure 6. The dark gray indicates steep gradients and high relative densities, while the light gray indicates weak density gradients and low relative densities. The density gradient plots are to be compared to the shadowgraphs near the triple point in Figure 6.

Figure 12

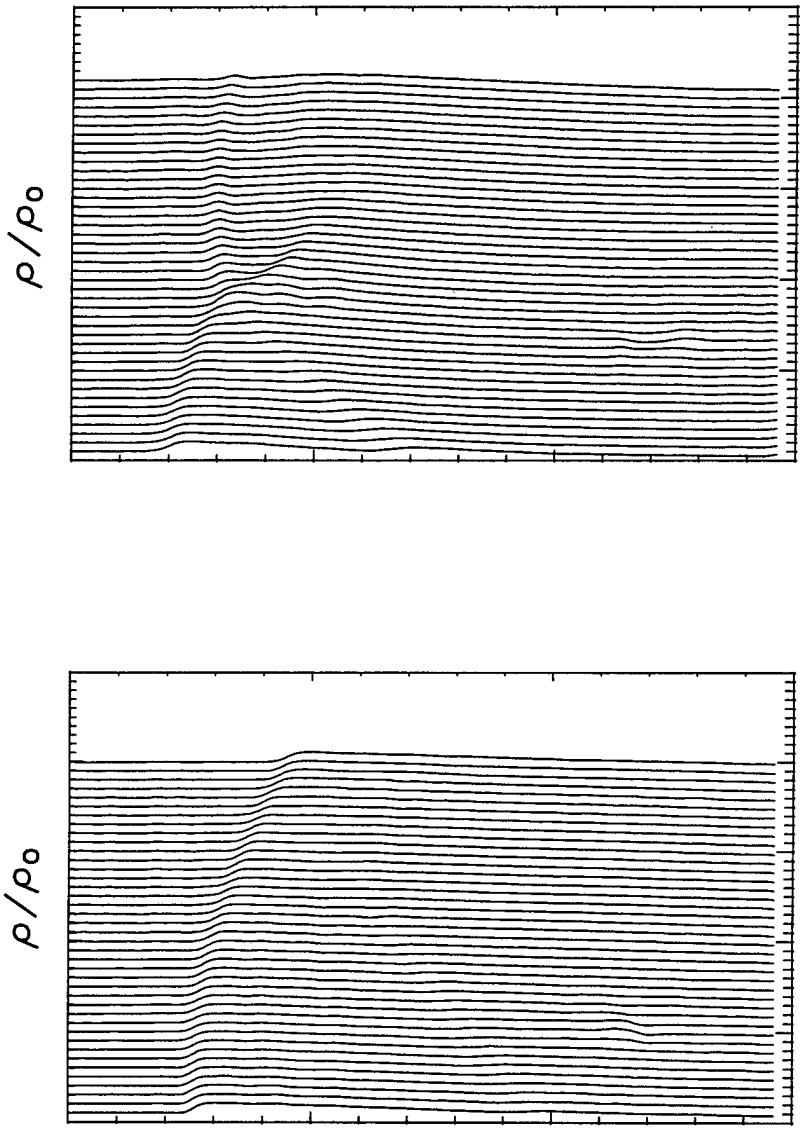

The relative density profiles ρ/ρ_0 as a function of radius (x-axis) and height above the plate (y-axis) at 10 and 30 μsec for shots without a thermal layer. The y-axis also measures the relative density; the spacing between tick marks is unity.

References

[1] *The effects of Nuclear Weapons*, Eds. S. Glasstone and P.J. Dolan (United States Department of Defense and the Energy Research and Development Administration, Washington DC, 1977).

[2] V.I. Artem'ev, V.I. Bergel'son, S.A. Medvedyuk, I.V. Nemchinov, T.I. Orlova, V.A. Rybakov, and V.M. Khazins, Fluid Dynamics 32, pg. 121 (1996); references therein.

[3] P.E. Alexandrov, Journal of Engineering Physics and Thermophysics 64, pg. 444 (1993).

[4] I.V. Nemchinov, V.I. Artem'ev, V.I. Bergelson, V.M. Khazins, T.I. Orlova, and V.A. Rybakov, Shock Waves 4, pg. 35 (1994).

[5] V.I. Artem'ev, I.E. Markovich, I.V. Nemchinov, and V.A. Sulyaev, Sov. Phys. Dokl. 32(4), pg. 245 (1987); V.I. Artem'ev, V.I. Bergel'son, S.A. Medvedyuk, I.V. Nemchinov, T.I. Orlova, V.A. Rybakov, and V.M. Khazins, Fluid Dynamics 32, pg. 121 (1996).

[6] L.F. Henderson, P. Colella, and E.G. Puckett, J. Fluid Mech. 224, pg. 1 (1991); G.P. Schneyer and D.E. Wilkins, *Thermal Layer-Shock Interaction (Precursor) Simulation Data Book*, S-Cubed Report SSS-R-84-6584, March 1, 1984; J.R. Barthel, C.E. Needham, T.H. Pierce, and G.P. Schneyer, *A Computational Model for Precursed Airblasts over Rough Surfaces*, Defense Nuclear Agency Report DNA-TR-89-244, November,1990; A.M. Abd-El-Fattah, L.F. Henderson, and A. Lozzi, J. Fluid Mechanics 76, pg. 157 (1976); H. Reichenbach, *Laboratory-Scale Airblast Precursor Experiments*, Vol. III, Defense Nuclear Agency Report DNA-TR-85-352-V3 (1989).

[7] B.H. Ripin, A.W. Ali, H. Griem, J. Grun, S. Kacenjar, C.K. Manka, E.A. McLean A.N. Mostovych, S.P. Obenschain, J.A. Stamper, in *Laser Interaction and Related Plasma Phenomena*, Vol. 7, pg. 857, eds. H. Hora and G.H. Miley editors, (Plenum Press, NY, 1986).

[8] J. Grun, J. Stamper, J. Crawford, C. Manka, B.H. Ripin, in *Laser Interactions and Related Plasma Phenomena*, Vol.9, eds. H. Hora and G. Miley (Plenum Press NY, 1990).

[9] J. Grun, J. Stamper, C.K. Manka, J. Resnick, R. Burris, and B.H. Ripin, Appl. Phys. Lett. 59 (2), pg. 246 (1991).

[10] Technically, the image intensity variations are proportional to fluctuations in the square of the index of refraction.

[11] *American Institute of Physics Handbook*, D.E. Gray, Coordinating Editor (McGraw-Hill, New York, 1957), pg. 6-21; The Argon index of refraction at 532nm is extrapolated from the handbook value at 589.6 nm assuming its behavior with wavelength is similar to that of Air, Oxygen, Nitrogen and Hydrogen, for which the index of refraction at a few wavelengths is given.

[12] R.B. Kennard in *Temperature, Its Measurement and Control In Science and Industry,* American Institute of Physics (Reinhold, New York, 1941).

[13] L.I. Sedov, *Similarity and Dimensional Methods in Mechanics*, translation by M. Friedman, M. Holt, ed., pages 210-233, (Academic, New York, 1959).

[14] The constant α was calculated by Sedov (ibid.), who solved the equations of motion in 1-D spherical geometry for given values of the adiabatic index γ. (Dependence on γ is the result of energy being tied-up in excited or ionized states and, therefore, not available to produce pressure.) For typical values of γ, such as 5/3, 7/5, and 6/5, α was determined to be 0.47, 0.84, and 1.7 respectively. In our experiment, if all of the laser energy is transformed into explosion energy then $\alpha \sim 2$. But if only 85% of the laser energy is absorbed by the mylar target then α would be 1.7, implying a post-shock γ of 6/5. Laser absorption of 85% is consistent with literature on the absorption of laser light by solid targets. (ex: B.H. Ripin, et al., Phys. Fluids 23, pg. 1012 (1980))

[15] For example see V.I. Bergel'son, I.V. Nemchinov, T.I. Orlova, V.A. Smirnov, and V.M. Khazins, Sov. Phys. Dokl. 32, pg. 691, 1987.

[16] *Holographic Interferometry*, C.M. Vest, (Wiley, New York, 1979).